CONF-871036--12

CONF-871036--12

DE88 002966

CERAMIC BREEDER MATERIALS

C. E. Johnson
Argonne National Laboratory, Argonne, Il 60439 USA

K. R. Kummerer
Kernforschungszentrum Karlsruhe, F.R. Germany

E. Roth
Commissariat a l'Energie Atomique, CEN Saclay, France

ABSTRACT

Ceramic materials are under investigation as potential breeder material in fusion reactors. This paper will review candidate materials with respect to a) fabrication routes and characterization, b) properties in as-fabricated and irradiated condition, and c) experimental results from laboratory and in-pile investigations on tritium transport and release. Also discussed are the resources of beryllium, which is being considered as a neutron multiplier. The comparison of ceramic properties that is attempted here aims at the identification of the most-promising material for use in a tritium breeding blanket.

1. INTRODUCTION

Current fusion reactor designs include a tritium breeding blanket for production of tritium. To be considered, a candidate material must a) release tritium, b) exhibit thermophysical, chemical, and mechanical stability at high temperature, c) be compatible with other blanket and structural materials, and d) possess desirable irradiation behavior. Lithium, in some form, is the only material suited for this task. Present candidates for the breeding material are liquid lithium and its alloys and certain lithium-containing solids,

Work supported by the U.S. Department of Energy, Office of Fusion Energy, under contract no. W-31-109-Eng-38.

principally the lithium-containing ceramics. This paper will focus only on the latter materials, namely, the oxide, γ-aluminate, silicate, and zirconate of lithium.

In materials evaluation, tabulations of properties data are critically examined. Table I lists the melting point (T_m), lithium atom density (ρ_{Li}), bulk density (ρ_{TD}), thermal conductivity (K), operating temperature range, and tritium solubility of the candidate materials. The lower operating temperature limit is based upon estimates of tritium diffusion, and the upper temperature limit is based upon thermal sintering or restructuring effects. A high tritium solubility can be detrimental because it indicates potential for high blanket inventory. A high lithium atom density and thermal conductivity, wide operating temperature range, and low tritium solubility are all favorable quantities. Accordingly, Li_2O appears favorable because of its high lithium atom density and thermal conductivity and its low tritium solubility; $LiAlO_2$ appears almost as favorable because of its broad operating temperature range. Except for Li_2O, all other candidates are certain to require a neutron multiplier due to their low lithium atom density.

Comparisons of the candidates can also be made by examining the rate of change with temperature in the value of a given property. Figure 1 displays the rates of change of several properties as a function of temperature. The figure is intended only to show trends to achieve acceptable performance; no attempt has been made to quantify the axes. The steepness of the slopes for a given property is intuitive and will only be firmly established once data become available. Performance must be considered to represent a measure of the overall operating performance of a given breeder material. A most interesting aspect of this figure is that tritium diffusion is the only property exhibiting a positive response to temperature.

Transformation of materials during neutron irradiation must also be considered because the neutron capture process eliminates one chemical component (Li) and produces others (T,He). These compositional changes can lead to the formation of second phases either as internal precipitates or as solid solutions. The impact of a change in composition for a ternary oxide is likely to be reflected in changes in its properties, e.g., melting point, tritium diffusivity, thermomechanical performance. Further, in any detailed evaluation of candidate blanket materials, strong consideration must be given to their tritium breeding potential. Currently, blanket designs use beryllium for neutron multiplication to ensure an adequate tritium breeding ratio (tritium atoms produced per fusion neutron).

The performance parameters considered are not of equal importance. The tritium breeding ratio is a key parameter since tritium self-sufficiency is a necessary requirement. A key safety concern is the tritium inventory within the blanket. The large uncertainty in tritium-related properties makes data comparisons difficult. In this paper, we assess the candidate materials based upon possible fabrication routes, their properties in the as-fabricated and irradiated condition, and experimental results from laboratory and in-pile investigations on tritium transport and release.

2. FABRICATION OF BREEDER MATERIAL COMPOUNDS

The geometrical shape of the ceramic breeder body depends on the design concept chosen for the breeder blanket module. There are several configurations for solid breeders: monolithic block, pressed and sintered pellets or plates, and spherical (or sphere pac) particles [1-3]. Thermal stress-induced cracking and fragment relocation impose difficulties in precise temperature control of monolithic blankets. To overcome the cracking problem

and its associated gap conductance uncertainties, blanket designs can employ either pressed and sintered plates or the sphere-pac configuration. With the BIT (Breeder in Tube) concept, the lithium ceramic is embedded within a cladding, e.g., as cylindrical pins, being cooled from outside. With the BOT (Breeder Out of Tube) concept, the situation is the reverse: the coolant is in tubes that penetrate the breeder. Hence, the geometry of the breeder ceramic is the pellet shape for the BIT concept and a sphere-pac for the BOT concept. The fabrication of ceramic breeders into the desired form needs to be demonstrated. Attention also needs to be placed on microstructural tailoring (e.g., controlled density, grain size, pore morphology), on impurities, and on stability to ensure the development of solid breeders with superior properties.

For material fabrication, two processes are to be considered: a) the chemical conversion of the commercially available source material (Li_2CO_3 or LiOH) into the desired oxide, and b) the compaction of the powder to the desired shape.

The preparation of sinterable powders from Li_2CO_3 and LiOH source material is schematically presented in Fig. 2. The "wet processes" (spray-drying) avoid introduction of impurities in the course of the dry milling step. The source materials normally contain lithium with natural isotopic composition, i.e., 7.5% Li-6 and 92.5% Li-7. For experiments that require other isotopic enrichments, either depleted or increased Li-6 content, Li_2CO_3 source material is available from special isotope suppliers.

The fabrication of lithium aluminate aims at producing the high-temperature γ-$LiAlO_2$ phase. This phase is also metastable at low temperatures. In a dry process [4] Li_2CO_3 and Al_2O_3 powders are milled together and heated to 700°C. At this temperature, a slow reaction leads to

formation of the denser α-phase material, which is completely transformed into the γ-phase at temperatures above 900°C. Different variants of this dry process have been established [5]. Also, the preparation of γ-$LiAlO_2$ from liquid mixtures of aluminum and lithium salts, as well as from pasty mixtures of Al_2O_3 and lithium salts, was examined [6]. In the wet process, aluminum metal chips are dissolved in aqueous LiOH solution, spray-dried, and calcined at 900°C to a sinterable γ-$LiAlO_2$ powder [7].

γ-$LiAlO_2$ in the sphere-pac configuration has been prepared: (1) by spray-drying of lithium aluminate sols [7a,7b], (2) by microwave denitration of the lithium aluminum sol solution [7a], or (3) by agglomeration of oxide powders [7d]. With the sphere-pac process, high density ceramic spheres are produced. Characteristically, three sizes of spheres of diametral ratios of 40:10:1 are used to achieve about 88% smear density (actual diameters are 1200, 300 and 30 μm). The spray drying of lithium aluminum sols was found to give good results [7a,7b]; however, the Li/Al stoichiometry frequently varied. The flow-sheet for large scale (kilograms) production by this promising method is still under examination. In the microwave dehydration denitration of the lithium-aluminum sol solution [7c], energy of kilohertz frequency heats the solution leaving the precipitated oxide particles cold. Nitrate elimination occurs at 600-650°C leaving a powder of 20 m^2/g surface area.

There are several silicates of lithium to be considered. The metasilicate (Li_2SiO_3) and the orthosilicate (Li_4SiO_4) are well known and thoroughly investigated. As recently demonstrated, Li_6SiO_5 exists under certain conditions [8,9] but is difficult to prepare and has a very limited stability range.

A standard method for the synthesis of Li_2SiO_3 is the co-milling of Li_2CO_3 with highly reactive SiO_2 powder in an aqueous mixture followed by heat treatment between 500° and 750°C for many hours [10-12]. Different intermediate drying techniques, e.g., spray-drying or slowly drying in a kneader, lead to powders of quite different sinterability. Final reaction products often require repeated milling and calcining. The lengthy milling may also cause an increased impurity level. All these drawbacks may be avoided by a recently developed wet chemical process that starts with LiOH [7,13]. In this process, a LiOH solution is slowly fed into a highly dispersed aqueous suspension of SiO_2. A final spray-drying and calcining at 600°C lead to a sinterable Li_2SiO_3 powder.

The lithium orthosilicate can be synthesized in a manner similar to the wet process for Li_2SiO_3[12]. The starting mixture, of course, contains correspondingly more LiOH according to the required stoichiometric relationship. In the initial precipitation step, Li_2SiO_3 is formed with excess LiOH; the remaining hydroxide is either oxidized to Li_2O_2 by introduction of H_2O_2 or transformed to dispersed carbonate by CO_2. The concluding calcining step at 600°C results in sinterable Li_4SiO_4 powder. Without this step, the final product would be quite coarse and have very limited sinterability. In addition to this wet process, dry mixing and calcining in vacuum at very high temperatures have been successfully applied [5]. Other wet processes using alcohol instead of water [8] also seem attractive. Specially doped orthosilicates (with Al and P ions) have been prepared by suspension in alcohol [14]. Also an organometallic process [15] resulted in a very fine grained Li_4SiO_4 powder.

For the fabrication of Li_2O several methods are applicable. In a customary process, the source material (Li_2CO_3) is calcined in vacuum and

ball-milled to a sinterable powder [5]. A more favorable process, as far as the impurity content is concerned, starts with an aqueous LiOH solution followed by precipitation of the peroxide (Li_2O_2) with H_2O_2, which is converted to sinterable Li_2O powder [16] by vacuum-calcining at 300-400°C.

A similar procedure is used for the preparation of Li_2ZrO_3. The intermediate compound Li_2O_2 is mixed with ZrO_2 powder and calcined at 900°C [16]. A preparation by the organometallic process mentioned above [15] has also been reported.

The quality of a sinterable powder is primarily defined by its specific surface area. For example, Li_2SiO_3, produced by spray-drying (Fig. 3) is easily processed to yield homogeneous ceramic compacts [13]. To obtain open pore structures, further preparational steps like granulation and subsequent calcination are necessary.

For compaction of the ceramic powder to molded solids, different procedures are applicable, especially a) cold-pressing and sintering, b) precompacting and hot isostatic pressing, c) extrusion, granulation, and sintering, and d) melting, liquid drop formation, and solidification. These procedures, as shown in the scheme of Fig. 4, result either in pellets or in spherical particles.

The simple procedure of cold-pressing and sintering is commonly used in mass production of ceramic materials. The sintering temperature varies between 800° and 1100°C and is an important factor for controlling the pellet structure. The sintering time is on the order of 5 hours, depending on preconditioning of the powder.

Hot pressing in a temperature range between 500° and 900°C may lead to compacts of very high density. In this more expensive process, the original grain size of the powder will not increase due to the lower temperature and the short exposure time [12].

The fabrication of spherical particles can be carried out by the granulation of extruded material. Ideal spherical shapes could be obtained by melting and freezing. However, free flowing particle beds are normally desired because they can be formed satisfactorily using "pebbles" of irregular size.

In qualification of the fabricated ceramic breeder, the following factors are important: shape (dimensions), density, chemical composition, isotope content, impurity content, crystallographic phases, and microstructure of the solid. The geometry and density of pellets, together with the theoretical density of the compound, can be used to derive a direct measure for the average porosity. The open porosity is measured by mercury porosimetry and can be correlated to the effective intrusion channel diameter. The latter can be evaluated from the cumulative open porosity by a modeling calculation. The chemical and isotopic composition of the ceramic is determined by routine analytical methods. The crystallographic structure is determined by X-ray diffractometry. The microstructure is primarily characterized by the "internal geometry" of the ceramic solid, which is highly important for tritium transport and also for mechanical strength [17]. The microscopic grain structure is visualized by ceramographic investigations. In this context the grain size and shape are important because they relate to transport and release of tritium. The adsorption of tritium on internal surfaces of the ceramic can be responsible for retention of tritium. Ceramographic structural data can be converted to the relevant specific surface area within the ceramic solid using simple modeling methods.

3. MATERIALS PROPERTIES

Properties data presented in this chapter are based on comparative measurements from various studies [18-21]; a rigorous comparison and

assessment of candidate material can only be achieved using values measured under comparable conditions and on comparable specimens. The impact of microstructure and impurities on properties, on material stability, and on performance of ceramics has long been recognized [22]. For example, porosity, pore morphology, and grain size have profound effects on thermal conductivity, mechanical properties, stability, and tritium inventory. Impurities can affect thermodynamic and chemical properties as well as transport behavior. The thermodynamic, thermophysical, and mechanical properties for the as-fabricated ceramic materials, as well as their irradiation behavior, largely determine design guidelines.

3.1 Thermodynamic Properties

Measurements have been made of the solubility of hydroxide in Li_2O and of the vaporization of hydroxide from Li_2O into a helium gas stream containing varying amounts of H_2O vapor [23-24]. The solubility data were used to enable corrected thermodynamic calculations (corrected for non-ideality of solutions of hydroxide in Li_2O) to be made on the Li_2O system [24a].

A general conclusion from the calculations is that the behavior of breeders will be strongly dependent on the oxygen activity prevailing in the system. Oxygen activity controls the form of the released tritium, i.e., either the oxidized or reduced form, the amount of tritium retained in the condensed phase, and the amount of blanket transported as LiOH/LiOT vapor. The sensitivity to oxygen activity in determining either oxidized or reduced forms of released tritium is such that nominally "pure" sweep gas containing only parts per million levels of oxygen and/or H_2O will be strongly on the oxidizing side. If oxygen activity is reduced sufficiently, it is possible for hydride (tritide) to become an important species in the condensed phase [25,25a].

Thermodynamic calculations have been carried out in detail for the condensed and gaseous phases for the breeder materials Li_2O, $LiAlO_2$, and Li_4SiO_4. From this work, a comparison of predicted thermochemical performance emerged. This comparison was based on the amounts of tritium retained in the condensed phase, the amount of tritium in the gas phase, the amount of elemental lithium vaporized, and the amount of LiOH vapor transport. The calculations suggest that the performance of $LiAlO_2$ is better than that of Li_2O, which, in turn, is better than that of Li_4SiO_4. At high temperatures and very low oxygen activities, Li_2O would be better than $LiAlO_2$ in respect to tritoxide retention in the condensed phase [25].

Partial pressures of the gaseous tritium-containing species T_2 and T_2O were calculated over Li_2O, Li_4SiO_4, and $LiAlO_2$ at 900 K and 1300 K for the oxygen activity range 10^{-25}-10^{-5}. Results show that both T_2 and T_2O partial pressures are greater over $LiAlO_2$ than over Li_2O and Li_4SiO_4 at both temperatures in the oxygen activity range 10^{-20}-10^{-5} [25].

Vaporization data for several candidate breeder materials have been reported [18,25b]. Partial pressures of the different species over the ceramics have been expressed as a function of temperature and different structural metals showing that higher lithium vapor pressures exist for materials with higher lithium content. Measurements made using a carrier gas stream of varying H_2O partial pressure showed that moisture enhances the volatility of Li_2O as LiOH [25b]. Results are presented in Fig. 5 derived from [25b,26] in terms of the equilibrium constants for the reaction $Li_2O(s) + H_2O(g) = 2\ LiOH(g)$.

In the FUBR 1A experiment, lithium transport from the ceramic pellets to the capsule walls was investigated [27]. Four materials, namely,

Li_2O, γ-$LiAlO_2$, Li_4SiO_4, and Li_2ZrO_3, were irradiated at 500-900°C in EBR-II. Temperature differences in the helium-filled pellet cladding gap were ~300°C at 900°C, ~155°C at 700°C, and less than 40°C at 500°C. The fractional lithium transfer was found to be temperature dependent. It was significant for Li_2O at all temperatures, reaching 1 at.% at 900°C, the largest observed for any material. No lithium transport was detected from the $LiAlO_2$ and Li_2ZrO_3 pellets but a slight amount of transport was detected from the Li_4SiO_4 pellets.

3.2 Thermophysical Properties

The most complete study of thermal conductivity for Li_2O and Li_2ZrO_3 as a function of porosity and temperature is reported in [28]. A comprehensive comparison of this property for materials of 80% T.D. is reported in [19] and presented in Fig. 6. These results show decreasing conductivity with increasing temperature; the order among solids is $Li_2O > LiAlO_2 > Li_4SiO_4 > Li_2ZrO_3$. Estimates have been made of thermal conductivity of 65% T.D. $LiAlO_2$ from the TRIO experiment [29,29a] and for sintered product and sphere-pac Li_2O and γ-$LiAlO_2$ [30]. The TRIO estimates showed little change from unirradiated values, while the sintered product and sphere-pac estimates showed significant change after irradiation. However, recent measurements on materials from FUBR-1 [31] showed essentially no change. Irradiation of $LiAlO_2$ to fluences of 10^{20} n cm^{-2} at temperatures to 750°C exhibited little change in thermal conductivity.

The differences between the thermal expansion of four solid breeders and two structural materials as a function of temperature are shown in Fig. 7 [32]. Li_2O exhibited the largest change, while γ-$LiAlO_2$ and Li_2ZrO_3 showed the smallest.

Thermal fracture studies for $LiAlO_2$ of several different geometries and at different temperature gradients showed better behavior for cylinders than that for disks. In the latter case the critical temperature difference was 400-500°C at about 600°C [33]. Dienst et al. [19] showed a critical temperature difference of 450-500°C for $LiAlO_2$ and $\lesssim$240°C for Li_4SiO_4; Li_2SiO_3 was found more resistant than $LiAlO_2$.

Sintering of the ceramic material is strongly temperature dependent, increasing with time and decreasing particle size. Stability tests (8 hours at 900°C) are reported in [32] (see Table II) for hot-pressed materials. The greatest changes were observed for Li_2O, somewhat smaller changes for Li_4SiO_4, and insignificant changes for Li_2ZrO_3 and γ-$LiAlO_2$. Annealing experiments were carried out on lithium aluminate for up to 40 days in air at 400-1100°C; dimensional, porosity, and weight changes were measured [33]. Lithium loss appears at ~850°C and shrinkage sets in at 900°C. Under identical conditions the behavior of Li_2SiO_3 and Li_4SiO_4 was poorer. No change of microstructure was observed for aluminates in the Alice 1 experiment up to 600°C and 10^{20} n cm^{-2} fluence, but sintering was detected in Alice 2 at irradiation temperatures of about 750°C for a 0.4 μm grain size material. In the low burn-up ($<$0.5 MW Yr/m^2) OG5 irradiation experiment, 70% T.D. Li_2O showed significant pore closure at temperatures above 850°C, whereas most pores remained open below 750°C. No pore closure was observed for 80% T.D. $LiAlO_2$ below 950°C [5].

3.3 Mechanical Properties

Elastic moduli reflect the atomic bond strength of materials and provide information on lattice defects. Young's modulus was measured as a function of porosity at room temperature on lithium oxide [34], on lithium aluminates [33], and on lithium metasilicate [19]; Young's modulus and shear

modulus were measured on 92% T.D. lithium oxide [35]. A comparison of Young's modulus of several breeders is displayed in Fig. 8 [19]. In the Alice 1 irradiation experiment on $LiAlO_2$ (fluence 10^{20} n cm^{-2}), no change in Young's modulus was detected at 400°C, but a 10% reduction was observed at 600°C [33]. No change was observed on lithium oxide specimens irradiated at 600°C [34].

Compressive strength was studied as a function of porosity and grain size and data are displayed in Fig. 9. Materials of low porosity and small grain size exhibit the greatest strength. No changes in compressive strength were noted for $LiAlO_2$ at 600°C for 1 at.% burn-up or up to 800°C for a 2 at.% burn-up. Compressive strength for $LiAlO_2$ with 75% T.D. and 0.4 μm grain size decreased from 275 MPa at 20°C, to 153 MPa at 500°C, and to 100 MPa at 900°C [33]. The compressive strength and bending strength of $LiAlO_2$ differ by a factor of 10. Bending strength of 80% T.D. aluminate, metasilicate, and zirconate (50-60 MPa) did not show significant change up to 600°C, but that of Li_2O began to decrease at 400°C [34]. For brittle materials, compressive strength is substantially larger than tensile strength, generally by a factor of eight. No direct measurements of tensile strength for the candidate materials are available. However, tensile strength was measured for $LiAlO_2$ and found to be ~0.1 that of compressive strength.

Creep rate at 10 MPa has been measured as a function of temperature and porosity for several materials [19,33] (see Fig. 10). The creep rate of Li_4SiO_4 was found to be about two orders of magnitude higher than that of Li_2SiO_3. The steady-state thermal creep rate for Li_2O was investigated as a function of stress (15-45 MPa) and temperature (700-800°C) [35]. From creep results, estimation was made of the dimensional and microstructure stability of breeder materials. Considered as rigid materials at creep rates of 10^{-6}/h and 10 MPa, temperature limits for 10 to 20% porosity material are: ~950°C for

$LiAlO_2$, ~825°C for Li_2SiO_3, ~750°C for Li_4SiO_4, and ~625°C for Li_2O. These limits were confirmed by experimental measurements for $LiAlO_2$ and Li_2SiO_3.

An attempt [19] has been made to assess the resistance of different breeder materials to thermal crack initiation. This assessment used a reduced parameter $k/E\alpha$, instead of the usual thermal shock parameter $\sigma_f k\ (1-\nu)/E\alpha$ (σ_f=tensile strength, k=thermal conductivity, ν=Poisson number, E=Young's modulus, α= thermal expansion). Results for 20% porosity materials, with α and k at 600°C and E at room temperature, are reported in Table III. The highest resistance to thermal crack initiation was found for $LiAlO_2$ and the lowest for Li_4SiO_4. For Li_2O, elastic and creep behavior indicates that it may be easily restrained by structural design [35].

3.4 Irradiation Behavior

Recent FUBR 1A irradiation tests tend to support the selection of upper temperature limits in Table I. Data indicate that tritium retention and pellet integrity are reasonably good [36-38]. Analysis of helium and tritium retention showed that Li_2O exhibits the greatest retention for helium, especially at the intermediate temperature (700°C), while tritium retention was lowest for Li_2ZrO_3. All four materials show an approximately linear proportionality for tritium and helium retention with burn-up. In the Alice experiments [39] tritium retention was strongly dependent on the nature of the structural material surrounding the sample during irradiation. Retention was much lower when surrounded by stainless steel rather than an aluminum-magnesium alloy.

The materials showed increase in fragmentation in the order Li_2ZrO_3, $LiAlO_2$, Li_2O, and Li_4SiO_4. $LiAlO_2$ at 95% T.D. was less fragmented than this same material at 85% T.D. Fragmentation was not burn-up dependent and was thought to result from thermal stresses arising from thermal gradients

and thermal expansion. In the Alice experiments, no significant fragmentation to $LiAlO_2$ was observed up to 600°C and 1 at.% burn-up; severe fragmentation was observed at ~750°C and thermal gradients of ~200°C/2.5 mm [33]. In the Exotic experiments, the integrity of specimens was generally good up to 600°C.

In the FUBR 1A experiment, swelling at 700 and 900°C was observed to be very low for 85% T.D. $LiAlO_2$ and Li_2ZrO_3, slightly higher for Li_4SiO_4, and rather high for Li_2O. Swelling was thought to arise from the retained helium in the material [38]. A small shrinkage was observed ($\lesssim$0.03%) for 75% T.D. $LiAlO_2$ in the Alice 1 experiment. No significant changes were noticed in grain growth for Li_2O, a slight growth for Li_4SiO_4, and no change for $LiAlO_2$ and Li_2ZrO_3 [38].

3.5 Material Compatibility

Compatibility studies have been carried out at 873 K between couples comprised of the breeder materials (Li_2O, $LiAlO_2$, and Li_2SiO_3) and the structural materials (Type 316 stainless steel, Incoloy 800, Inconel 25, HT-9, and Ti-6242) [40,40a]. Li_5FeO_4 and Li_2CrO_2 were common corrosion products. Similar studies [41,42] on the same ceramic materials and alloys at 873-973 K identified $Li_2Ni_8O_{10}$ as a corrosion product with Inconel-625. Of these breeder materials, Li_2O was most reactive and $LiAlO_2$ was least reactive. The corrosion chemistry of Li_2O has been established in a basic thermodynamic study [43,44]. Li_2O was found to be inert to the metals, provided it was rigorously freed of moisture impurity. Corrosion observed previously was attributed to LiOH contamination of Li_2O. Porter et al. [45] reported similar findings on long term studies of doped Li_2O (with H_2O) in contact with austenitic and ferritic alloys. Materials doped to 6% H_2O exhibited shallow attack (~3.4 μm) after 700 hrs at 873 K. Experiments on similar materials run for >2000 hrs exhibited identical behavior. The reaction rate between oxide

breeders and stainless steel cladding is shown in Fig. 11 [46]. Temperature limits can be derived from this figure for a 20 μm thick reaction zone after 100 h, i.e., 700°C for Li_2O, 900°C for L_4SiO_4, and 1000°C for Li_2SiO_3, $LiAlO_2$, and Li_2ZrO_3.

Compatibility studies between beryllium and Li_2SiO_3 at 600°C and 750°C show that reaction effects seem acceptable at 600°C but not at 750°C [46]. Studies of the compatibility between beryllium and $LiAlO_2$ at 600°C and 700°C for 1500 h show that beryllium undergoes no measurable oxidation under these conditions [47].

No reaction is expected between solid breeders and pure helium, only between solid breeders and coolant impurities, e.g., H_2O. Li_2O readily reacts with moisture to form LiOH. Sensitivity of $LiAlO_2$ to moisture has been investigated by Rasneur et al. [33]. Changes in weight and in phase for specimens exposed to a range of humidity levels were studied as a function of time; the phases LiOH 2 $Al(OH)_3 \cdot 2\ H_2O$ and $Li_2O \cdot H_2O$ were identified. In the presence of CO_2, the latter phase is transformed into Li_2CO_3. No alteration of aluminate is detected for relative humidity less than 25%. Similar tests carried out on Li_2SiO_3 showed comparable weight gain per surface area unit.

4. TRITIUM TRANSPORT AND RELEASE

In an operating fusion reactor, the tritium breeding blanket will reach a steady state in which the tritium release rate equals the production rate. The tritium release rate must be sufficient to ensure that the tritium inventory in the blanket does not become excessive. The kinetics that govern the transport and release of tritium from the breeder material must be fully understood if we are to establish optimum operating temperature limits for the blanket. Tritium generated within a candidate material undergoes a) diffusion to the crystal surface, b) surface reaction, c) desorption from the crystal

surface, and d) percolation through the pore structure. Thus, key parameters that must be investigated include tritium diffusion within the solid and desorption from the grain surface.

4.1 Tritium Release Experiments

In-situ tritium recovery experiments provide a method of evaluating the feasibility of the lithium ceramics as tritium breeders. Many experiments [29,48-58] have been performed to determine the tritium release rate. For some materials the rates have shown significant variance. Further, discrepancies in interpretation concerning the controlling mechanism for tritium release appear throughout the literature because of poor characterization of system variables e.g., grain size, extraction temperature, and carrier gas composition during extraction. These and other tritium control parameters were identified at a recent workshop [59] on tritium behavior.

Laboratory and in-situ tritium recovery experiments have focused on the release process with the objective of characterizing the rate-limiting phenomena. In-situ tritium recovery experiments have been conducted on Li_2O [48,49,49a] on $LiAlO_2$ [29] and on Li_2SiO_3/Li_4SiO_4 [55,56]. A striking feature of these in-situ release experiments is the ease with which tritium is released from the solid. Characteristically, tritium is observed in the purge gas stream within a few hours after irradiation was initiated. Further, residual tritium content in the solid has been found to be very low, indicative of low tritium solubility, and therefore, a potentially low inventory. Studies continue in order to rigorously define release parameters.

For the TRIO experiment [29], tritium recovery was readily achieved to temperatures as low as 770 K. In this experiment, it was found that the addition of H_2 to the purge gas stream significantly enhanced tritium release. This implies that surface processes play a significant role in the overall

release process. Throughout the course of the TRIO experiment, the predominant species evolved from the test capsule was the noncondensible tritium form (HT). In sealed capsule tests, where tritium is evolved by post-irradiation annealing, the HT fraction is generally only 1-10% of the total. Recent in-situ tritium recovery tests on Li_2O (VOM, CRITIC) also showed a very high fraction (~90%) of the condensible (HTO, T_2O) tritium species. The LILA-1 experiment in which $LiAlO_2$ was placed in quartz and stainless steel capsules showed the quartz capsule to release tritium predominantly in the condensible form, while the steel capsule released tritium in the noncondensible form. These data suggest the potential for immediate reduction of the released material on structural members.

Tritium diffusion data on various lithium ceramic breeder candidates have been tabulated from both laboratory and in-reactor release-type experiments. Much of the release data pertain to Li_2O [60-65]. Below about 400°C the activation energy varies between about 96 and 143 kJ (23 and 34 kcal) for four separate groups of data [60-63]. However, only one data set [63] exhibits the relatively large activation energy of about 143 kJ. The rest of the data [60-62] show activation energies clustering around 96 kJ. There are several data sets for tritium diffusion at 500-950°C. The activation energy in these data varies considerably from a low value of about 29 kJ (7 kcal) to 77 kJ (18 kcal) to a high value of about 116 kJ (28 kcal) [48,49,52]. The last two values are reasonably close to the low temperature ($\sim<400^{o}C$) results [44-46]. However, the low value of 29 kJ is consistent with the activation energies of deuterium and hydrogen diffusion in Li_2O [65-70].

There is considerable spread in the apparent activation energy for tritium diffusion in lithium ceramics. The reason for this is not understood

at present. Possible causes may include a) different experimental conditions (e.g., wet or dry), b) different sample characteristics (e.g., single crystal versus polycrystal, pellets, powder forms), and c) effects of other mechanisms besides bulk diffusion contributing to the tritium release process. There is also a wide spread in the absolute values of the derived diffusion coefficient D_T. For example, D_T (600°C) can range between a low value of 5×10^{-11} cm^2/sec [67] to a high value of 3.5×10^{-8} cm^2/sec [64]; but, as discussed before, this could be attributed partly to uncertainty in the sample characteristics.

4.2 Model Development

A computer program is being developed at Argonne National Laboratory to describe tritium behavior in ceramic breeder materials [71]. As presently constructed, the program focuses on modeling diffusion in the solid and desorption from the surface. The program is based on the solution [72] of the differential equation

$$\frac{1}{D}\frac{\partial C}{\partial t} = \frac{1}{r^2}\frac{\partial}{\partial r}\left(r^2 \frac{\partial C}{\partial r}\right) + \frac{G}{D}$$

where D is the diffusivity, C is the tritium concentration, r is the grain radius, G is the tritium generation rate. The equation for tritium release R_t is given by

$$R_t = 1 - \frac{3K_d}{Ga} C_1 \left[\frac{Ga}{3} - 2h^2 aG \sum_{n=1}^{\infty} \frac{\exp(-D\alpha_n^2 t)}{\alpha_n^2 [a^2\alpha_n^2 + ah(ah-1)]} \right] + K_d C_1$$

where

a = grain radius
K_d = effective first-order desorption rate constant
C_1 = tritium concentration evaluated at r=a prior to a temperature change
h = K_d/D
t = time

In this equation, α_n represents the roots of $a\alpha \cot a\alpha = 1-ah$. The release rate was calculated using the diffusion-desorption model, and the calculated results were compared to the observed tritium release rate for a sample of Li_2SiO_3 from the LISA-1 experiment. A typical plot is shown in Fig. 12. The model predicts the initial rise in release rate and the release rate after 100,000 seconds quite well but does a poorer job of predicting the release rate between 10,000 and 75,000 seconds. The calculated tritium release profile is also in good agreement with the observed data for time periods =following a large temperature decrease (~250,000, 450,000, and 675,000 sec) or increase (~350,000 sec). One shortcoming of the current model is that it uses a characteristic radius of the sample to calculate the release rate. The samples used in the LISA-1 experiments have a large distribution of grain sizes, and it is difficult to assign a characteristic grain size to the sample. Since the tritium release is dependent on the grain size, this could have a substantial effect on the release profile. To correct this shortcoming the model is being altered to allow for a distribution of grain sizes as input.

5. NEUTRON MULTIPLIERS

Aside from its neutronic properties, the neutron multiplier should be resistant to change during irradiation and be compatible with the surrounding materials. Neutronically, the elements Be, Bi, Pb, and Zr appear acceptable. However, beryllium is favored as the reference neutron multiplier because it combines excellent multiplication with low density, high specific heat, and high thermal conductivity. The main concerns for beryllium are irradiation swelling caused by helium generation, corrosion, and its limited resources.

5.1 Irradiation Behavior

Helium gas is generated in beryllium from the $(n,2n)$ and (n,α) reactions. Small grain size and high temperature will generally enhance helium release, thereby reducing the driving force for swelling. Post-irradiation annealing studies [73-76] of beryllium indicate that (1) there is a threshold temperature below which swelling is insignificant, and (2) there is a limit to volume increase (~30%) beyond which no further swelling occurs. The swelling threshold temperature depends on the helium gas content, decreasing with increasing neutron exposure. The maximum volume increase of 30% appears to be a geometrical limit at which the majority of the internal bubbles touch and release their gases. Such volume increases were only observed when the annealing temperatures are >1300 K.

5.2 Corrosion Behavior

The corrosion behavior of beryllium in oxygen, nitrogen, and water environments has been examined [77]. The reaction of beryllium with both oxygen and nitrogen follows the parabolic rate. Significant oxidation appears between 870 and 970 K and increases gradually up to 1100 K, after which the temperature of oxidation increases rapidly until actual burning commences at 1470 K. The reaction of beryllium with nitrogen follows the same pattern, but the reaction rates are lower. The corrosion of beryllium in high temperature water shows a wide variation in behavior. However, high purity beryllium in deionized water at 590 K exhibited corrosion rates of <20 mg/cm^2/mo. Beryllium can also interact with steel to form a hard surface coating. In particular, beryllium has a high affinity for nickel, and the compound NiBe predominates on the surface of high nickel steel. Other compounds which can form include $FeBe_2$ and BeC. The extent of the interaction with stainless steel should be small, however, at blanket operating temperatures.

5.3 Beryllium Resources

The availability of beryllium is summarized in Table IV, where U.S. Bureau of Mines (U.S.B.M.) and U.S. Geological Survey (U.S.G.S.) estimates are shown [78,79]. The Bureau of Mines data focused on the U.S. reserve and resources, and the Geological Survey data focused on the world-wide reserve and resources. The Bureau of Mines defines known resources of beryllium to consist primarily of bertrandite ($4BeO \cdot 2SiO_2 \cdot H_2O$) located at Spor Mountain and Gold Hill, Utah, and the Seward Peninsula, Alaska, and of beryl ($3BeO \cdot Al_2O_3 \cdot 6SiO_2$) located in the coarse-zoned pegmatites of New England, South Dakota, and Colorado. The Geological Survey estimates that about 725,000 MT of beryl is available in such deposits in North and South Carolina alone.

To address the resource issue, it is necessary to consider beryllium recycle [80]. With recycle, losses can be limited to the sum of recycle process losses and beryllium burn-up losses. Currently, powder metallurgical fabrication processes for sintered beryllium metal products result in an approximately 7% recycle process loss rate [81,82]. It is possible that, with sufficient incentive, this loss rate could be reduced to about 1%. The burn-up losses are likely to be small, but will compete with the recycle losses when recycle is very efficient. For extended service, efficient recycle is required and the recycle process losses must decrease as the multiplier thickness increases.

Thin multiplier coatings ($<$0.1 cm) are acceptable for intermediate term service without recycle. Even with 7% recycle losses, they are also acceptable for long term service. Thicker multiplier coatings (~1 cm) are acceptable for short term service without recycle, but require recycle for intermediate term service and efficient recycle for long term service. Thin

multipliers (~5 cm) are acceptable for short term service without recycle. They can qualify for intermediate term service with very efficient recycle (<1% loss/recycle). Thick multipliers (~10 cm) are unacceptable for short term service without recycle. Efficient recycle (<1% loss/recycle) may be sufficient for intermediate term service. Thick multipliers do not appear to offer potential for long term service.

Based upon these observations, it appears reasonable to consider beryllium multipliers for the first and second generations of fusion reactor service, but close attention to beryllium recycle losses will be required. Since the impurities in beryllium will activate in the fusion environment, a remote refabrication technology will be required [63,64]. Without very efficient recycle, thick beryllium multipliers should be considered for use only in the first generation of fusion reactors.

6. SUMMARY

In this assessment, one finds that the fusion community has given considerable attention to Li_2O, less attention to $LiAlO_2$ and Li_4SiO_4, and little attention to Li_2ZrO_3. The result is that the data base for these materials is very uneven, and rigorous comparisons are hard to make. Currently, effort is being directed to evening out the data base, especially with respect to Li_2ZrO_3. This material has shown excellent irradiation performance and is now receiving attention in laboratory studies and purge flow irradiation experiments. Table V lists the above named candidates and gives some indication of the breadth of the data base for each candidate.

Among the candidates, lithium oxide is highly regarded because of its high lithium atom content, low tritium solubility, high thermal conductivity, reasonably rapid tritium release, and high tritium recovery feasibility. It is probably the only material that could satisfy the tritium breeding

requirements without a neutron multiplier. Its principal disadvantage results from its high hydroxide/tritoxide and atomic lithium vapor pressure, which could result in transport of blanket material to cooler zones and closure of porosity. Lithium aluminate might be considered superior to Li_2O because of its better swelling resistance, higher melting point, broader operating temperature window, slow reaction with water, and its excellent irradiation behavior, especially for high density material (95% T.D.). However, its tritium diffusivity characteristics are poorer; therefore, this material requires a higher minimum operating temperature to maintain low tritium inventory. Li_4SiO_4 behaves much like Li_2O in many respects. It exhibits good tritium diffusivity and chemical stability. However, recent closed capsule irradiation test showed this material to fragment severely, probably due to thermal expansion. Li_2ZrO_3 has good stability and low tritium retention, and it has exhibited excellent irradiation characteristics. Its principal disadvantage is activation of zirconium under irradiation, which could cause maintenance problems. Fuller evaluation is hampered by a lack of data.

In summary, the materials may be ordered as follows: Li_2O, $LiAlO_2$, Li_4SiO_4, and Li_2ZrO_3. However, one must recognize the potential for reordering as the data base develops. Critical to a rigorous assessment are the tritium-related properties, e.g., solubility, release, diffusivity, and burn-up. Advanced methods of preparations of the four candidates may provide materials of superior performance and may affect their ranking. Further studies on the above materials appear warranted.

ACKNOWLEDGMENTS

We wish to acknowledge the help and assistance of Dr. N. Roux (CEA) in the preparation of this manuscript.

REFERENCES

1. C. Baker et al., Argonne National Laboratory Report, ANL/FPP-80-1 (1980).

2. M. Abdou et al., Argonne National Laboratory Report, ANL/FPP-82-1 (1982).

3. M. Abdou et al., Argonne National Laboratory Report, ANL/FPP-83-1 (1983).

4. E. Roth et al., Transactions ENC'86, Vol. 3, p. 145.

5. L. Yang, R. Medico, W. Baugh, and K. Schultz, J. Nucl. Mater. 103-104 (1981) 585.

6. B. Rasneur, Fusion Techn. 2 (1984) 1017.

7. D. Vollath, H. Wedemeyer, and E. Gunther, Fusion Techn. 2 (1984) 967.

7a. C. Alvani, S. Casadio, L. Lorenzini, and G. Brambella, Fusion Tech. in press.

7b. B. Palmer, Proc. Amer. Ceramic Society Mtg., Pittsburg, PA, 1987.

7c. M. Korzumi, et al., Nuclear Tech. 61 (1983) 55.

7d. B. J. F. Palmer, L. E. Bahem, and A. Celli, Amer. Ceramic Society Bul., 63 (1984) 1030.

8. D. Vollath and H. Wedemeyer, J. Nucl. Mater. 141-143 (1986) 334.

9. A. Skokan, H. Wedemeyer, D. Vollath, and E. Gunther, Fusion Techn. 2 (1986) 1255.

10. A. J. Flipot, P. Diels, and R. Lecocq, J. Nucl. Mater. 133-134 (1985) 226.

11. A. J. Flipot and P. Diels, J. Nucl. Mater. 141-143 (1986) 339.

12. F. Rigby and P. Kennedy, Fusion Techn. 2 (1984) 953.

13. D. Vollath, H. Wedemeyer, and E. Gunther, J. Nucl. Mater. 133-134 (1985) 221.

14. A. Skokan, D. Vollath, H. Wedemeyer, E. Gunther, and Werle, This conference.

15. D. J. Suiter, J. W. Davis, and B. A. Kirkpatrick, J. Nucl. Mater. 103-104 (1981) 579.

16. P. Kennedy, K. E. Gilchrist, D. E. Walker, and S. Broughton, Fusion Techn. 2 (1986) 1013.

17. H. Elbel, This conference.

18. D. Suiter, "Lithium Based Oxide Ceramics for Tritium Breeding Applications," Report MDC E 2677 UC 20 (June 1983).

19. W. Dienst, "Properties and Comparison of Ceramic Oxide Breeder Materials for Fusion Reactors," This conference.

20. C. Denuziere and N. Roux, "Data and Properties of Aluminate $LiAlO_2$," CEA/NET Contract No. 5/FU-F/NET (November 1984).

21. A. Skokan, H. Wedemeyer, D. Vollath, and E. Gunther, Proc. 14th Symposium on Fusion Technology, Avignon, 1986 (Pergarmon Press, Brussels, 1986), p. 1255.

22. W. D. Kingery et al., Introduction to Ceramics, 2nd Ed., John Wiley and Sons (1976).

23. J. H. Norman and G. R. Hightower, J. Nucl. Mater. 122&123 (1984) 913.

24. M. Tetenbaum and C. E. Johnson, J. Nucl. Mater. 126 (1984) 25.

24a. M. Tetenbaum, A. K. Fischer, and C. E. Johnson, Fusion Tech. 7 (1985) 53.

25. C. E. Johnson and A. K. Fischer, J. Nucl. Mater. 130 (1985) 445-453.

25a. A. K. Fischer and C. E. Johnson, Proc. Amer. Ceram. Soc. Mtg., Pittsburg, PA, April 1986.

25b. M. Tetenbaum and C. E. Johnson, J. Nucl. Mater. 120 (1984) 213.

26. Y. Tanaka, T. Suzuki, S. Mori, et al., Fusion Tech. 8 (1986) 947-952.

27. G. W. Hollenberg, D. L. Baldwin, R. Wisner, and B. Carlson, Proc. Intl. Symp. on Fusion Reactor Blanket and Fuel Cycle Technology, Tokai-Mura, 1986, p. 90.

28. T. Takahashi and T. Kikuchi, J. Nucl. Mater. 91 (1980) 93.

29. R. G. Clemmer et al., J. Nucl. Mater. 133&134 (1985) 71.

29a. S. W. Tam et al., J. Nucl. Mater. 133&134 (1985) 234.

30. Y. Y. Liu and S. W. Tam, Fusion Techn. 7 (1985) 30.

31. J. L. Ethridge and D. E. Baker, "Effects of Fast Neutron Evaluation on Thermal Conductivity," Proc. of Pittsburg Conference, April 1987.

32. D. L. Smith et al., "Blanket Comparison and Selection Study," ANL/FPP84-1 (1984) p. 6.3-30.

33. B. Rasneur, F. Botter, and M. Briec, "Ceramic Breeders - Report 1982 - 1986," CEA Note in press.

34. P. Kennedy, Proc. 14th Symposium on Fusion Technology, Avignon, 1986 (Pergamon Press, Brussels, 1986) p. 1013.

35. M. C. Billone, Y. Y. Liu, R. B. Poeppel, J. L. Routbort, K. C. Gorreta, and D. S. Kupperman, J. Nucl. Mater. 141-143 (1986) 282-288.

36. G. W. Hollenberg, "Pellet Integrity and Swelling of Lithium Ceramics," HEDL 7643 (1987).

37. G. W. Hollenberg, "Swelling of Lithium Ceramics During Irradiation," Proc. Pittsburgh Conference, April 1987.

38. G. W. Hollenberg and D. L. Baldwin, J. Nucl. Mater. 133&134 (1985) 242.

39. J. P. Bonal, "Mesures Post Irradiatoires des Quantites Residuelles de Tritium et d'helium 4 dans l'aluminate de lithium $LiAlO_2$," Memoire du Conservatoire National des Arts et Metiers (1987).

40. P. A. Finn, S. R. Breon, and N. R. Chellew, J. Nucl. Mater. 103&104 (1981) 561.

40a. O. K. Chopra, T. Kurasawa, and D. L. Smith, Proc. Topical Conf. Ferritic Alloys for Use in Nuclear Energy Technologies, J. Davis and D. Michel, eds., Snowbird, Utah, June 19-23, 1983, p. 209.

41. H. Takeshita, T. Kurasawa, S. Muraoka, S. Nasu, M. Miyake, and T. Sano, J. Nucl. Mater. 80 (1979) 249-252.

42. T. Kurasawa, H. Takeshita, and S. Nasu, J. Nucl. Mater. 92 (1980) 67.

43. R. J. Pulham, W. R. Watson, and J. S. Collinson, J. Nucl. Mater. 122&123 (1984) 1243.

44. R. J. Pulham, W. R. Watson, and N. P. Young, Proc. 14th Symposium on Fusion Technology, Avignon, 1986 (Pergamon Press, Brussels, 1986) p. 963.

45. D. L. Porter, J. R. Krsul, M. T. Lang, L. C. Walters, and M. Tetenbaum, J. Nucl Mater. 122&123 (1984) 929.

46. P. Hofman and W. Dienst, "Compatibility Studies of Metallic Materials with Lithium-Based Oxides," This conference.

47. T. Flament, D. Herpin, P. Perodeaud, P. Fauvet, and J. Sannier, "Compatibility of Beryllium with Lithiated Ceramics and Stainless Steels," CEA Progress Report, 1986 (SCECF no. 55).

48. T. Kurasawa, H. Takeshita, and H. Watanabe et al., J. Nucl. Mater. 122&123 (1984) 902.

49. T. Kurasawa, H. Yoshida, H. Takeshita et al., J. Nucl. Mater. 133&134 (1985) 196.

49a. R. A. Verrall, J. M. Miller, and S. R. Bokwa, American Ceramic Soc. 89th Annual Meeting and Exposition, Pittsburgh, Penn., 1987 April 26-30; for publication in Advances in Ceramics.

50. E. Roth, J. J. Abassin, and F. Botter et al., J. Nucl. Mater. 133&134 (1985) 238.

51. H. Kwast, R. Conrad, and J. D. Elen, J. Nucl. Mater. 133&134 (1985) 246.

52. T. Kurasawa, H. Watanabe, and G. W. Hollenberg, J. Nucl. Mater. 141&142 (1986) 265.

53. M. Briec, F. Botter, and J. J. Abassin et al., J. Nucl. Mater. 141&142 (1986) 357.

54. H. Kwast, R. Conrad, and P. Kennedy et al., J. Nucl. Mater. 141&142 (1986) 300.

55. H. Werle, J. J. Abassin, and M. Briec et al., J. Nucl. Mater. 141&142 (1986) 321.

56. R. G. Clemmer, H. Werle, and M. Briec, Proc. Int. Symp. Fusion Reactor Blanket and Fuel Cycle Technology, Oct. 27-29, 1986 Tokai, Japan, p. 51.

57. T. Kurasawa, G. W. Hollenberg, and H. Watanabe, Ibid, p. 43.

58. H. Watanabe, T. Kurasawa, E. Roth, and D. Vollath, Ibid, p. 33.

59. I. Hastings, Ed., Modeling Workshop - Chalk River, April 1987.

60. H. Kudo and K. Okuno, J. Nucl. Mater. 101 (1981) 297.

61. K. Okuno and H. Kudo, Proc. Fall Meeting of Atomic Energy Soc. of Japan, F-17 (1981).

62. S. Nasu, H. Kudo, K. Shiozawa, T. Takashashi, T. Kurasawa, M. Tachiki, and K. Tanaka, J. Nucl. Mater. 68 (1977) 261-264.

63. V. G. Vasilev, S. R. Borisov, N. N. Riazantseva, and A. A. Vashman, US/USSR Workshop on Engineering and Economic Problems of ETF, Moscow and Leningrad (USSR), September 1979.

64. K. Okula and D. K. Sze, "Tritium Recovery from Solid Breeders: Implication of the Existing Data," UWFDM-351, presented at the ANS Conf. on Tritium Technology in Fission, Fusion and Isotopic Applications, April 29-May 1, 1980, Dayton, OH.

65. J. Shearer, S. W. Tam, and C. E. Johnson "Tritium Diffusion in Lithium Oxide Solid Breeder Materials," Trans. Amer. Nucl. Soc. 44 (1983) 310.

66. D. Guggi, H. R. Ihle, and U. Kurz, Proc. 9th Symposium on Fusion Technology, Grarmisch-Partinkirchen (FRG), June 1976, p. 337-334.

67. D. Guggi, H. R. Ihle, D. Bruning, U. Kurz, S. Nasu, K. Noda, and T. Tanifuji, J. Nucl. Mater. 18 (1983) 100-108.

68. T. Tanifugi, K. Noda, T. Takahashi, and H. Watanabe, J. Nucl. Mater. 149 (1987) 227.

69. R. Wiswall and E. Wirsing, BNL-50748 (1977).

70. H. Katsuta, S. Konishi, and H. Yoshida, Proc. Fall Meeting of Atomic Energy Soc. of Japan, F-16 (1981).

71. J. P. Kopasz, S. W. Tam, and C. E. Johnson, This conference.

72. H. S. Carslaw and J. C. Jaeger, Conduction of Heat Solids, 2nd Edition, p. 245.

73. J. B. Rich, G. B. Redding, and R. S. Barnes, J. Nucl. Mater. 1 (1959) 96-105.

74. C. E. Ells and E. C. W. Perryman, ibid, 73-84.

75. J. R. Weir, Proc of Inter. Conf. on the Metallurgy of Beryllium, Institute of Metals, London, Oct. 16-18, 1961, pp. 362-371.

76. J. B. Rich, G. P. Walters, and R. S. Barnes, J. Nucl. Mater. 4, (1961) 287-294.

77. C. R. Tipton, Editor, Reactor Handbook, Vol. 1 - Materials, Interscience Publishers, Inc., New York (1960).

78. D. Petkof, "Beryllium," Mineral Facts and Problems, U.S. Bureau of Mines Bulletin 650 (1980).

79. W. R. Griffitts, "Beryllium," U.S. Geological Survey Prof. Paper 820 (1973).

80. D. H. Berwald and S. Zenczak, Fusion Tech. 8 (1985) 1143.

81. J. D. Lee et al., "Feasibility Study of a Fission-Suppressed Tandem Mirror Hybrid Reactor," Lawrence Livermore National Laboratory, UCID-19327 (1982).

82. D. H. Berwald et al., "Fission Suppressed Hybrid Reactor - The Fusion Breeder," Lawrence Livermore National Laboratory, UCID-19638 (1982).

Table I. Property Values and Temperatures for Candidate Solid Breeder Materials

Breeder	Properties				Operating Temperature Range, K	Tritium Solubility[a]
	T_m, K	ρLi_4 g/cm^3	ρTD_4 g/cm^3	K, W/mK		
Li_2O	1706	0.93	2.01	3.4	673 - 1073	L
$LiAlO_2$	1883	0.27	2.61	2.2	723 - 1473	L
Li_2SiO_3	1473	0.36	2.53	1.5	683 - 1073	H
Li_4SiO_4	1523	0.54	2.35	1.5	583 - 1223	M
Li_2ZrO_3	1888	0.33	4.15	1.3	673 - 1673	M
Li_8ZrO_6	1568	0.68	2.99	1.5	623 - 1253	M

[a] L= low, M = moderate, H = high

Table II. Thermal Stability Test

Material	Weight Loss, %	Dimensional Change, %	Grain Growth, μm Before/After
γ-$LiAlO_2$	0.04	0.00	<1/<1
Li_2ZrO_3	0.08	-0.03	2/2
Li_4SiO_4	0.3	-0.74	2/20
Li_2O	1.34	-2.4	6/80

Table III. Properties of Ceramic Breeder Materials (of 80% T.D.) Relevant to Thermal Crack Formation

Material	k (600°C) W/mK	α (600°C) 10^{-5}/K	E (R.T.) GPa	$K/E \cdot \alpha$ 10^{-6} m^2/s
Li_2O	3.5	3.3	70	1.5
$LiAlO_2$	2.6	1.2	80	2.7
Li_2SiO_3	2.0	2.1	55	1.7
Li_2ZrO_3	1.4	1.1	70	1.8

Table IV. World Beryllium Resources
(Metric Tons of Contained Beryllium)

	Reserves	Other	Total
North America			
United States	25	48	73
Canada	--	23	23
Mexico	--	2	2
South America			
Argentina	25	47	72
Brazil	140	256	396
Asia: India	64	119	183
Africa			
Mozambique	6	11	17
Rwanda	11	20	31
Republic of South Africa	15	29	44
Uganda	15	26	41
Zaire	7	14	21
Europe: U.S.S.R.	61	111	172
Oceania: Australia	11	19	30
World Total	380	725	1105

Table V. Assessment Tabulation

	Li_2O	$LiAlO_2$	Li_4SiO_4	Li_2ZrO_3
H_2O adsorption/desorption	0	00 XX	0	0
Hydrogen adsorption/desorption	0	0	0	0
Tritium diffusion	00 XX	00	00 XX	0
Tritium release	00	00	00	0
Chemical stability	00 XX	00 XX	00 XX	00 XX
Compatibility with Be	0	00 XX	0	0
Compatibility with Structural	00 XX	00 XX	00 XX	00 XX
Irradiation stability	00 XX	00 XX	00 X	00 XX
Thermal conductivity	00 XX	00	00	00
Thermal Expansion	00	00	00	00
Achievable bulk density	00	00	00	00
Operating temperature window	00	00	00	00

0 = results not available
00 = results available
X = results unfavorable
XX = results favorable

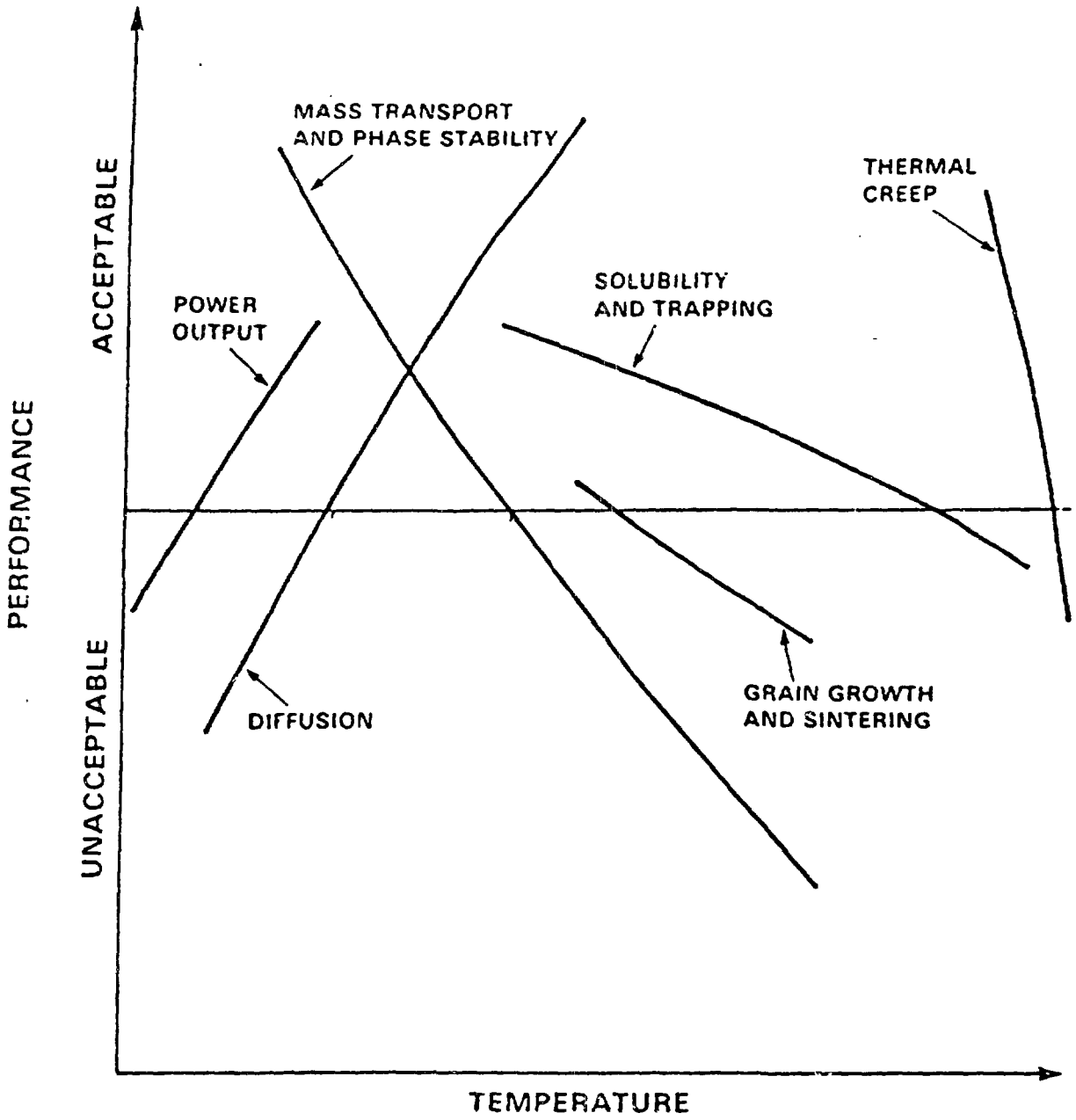

Fig. 1. Breeder Material Properties as a Function of Temperature

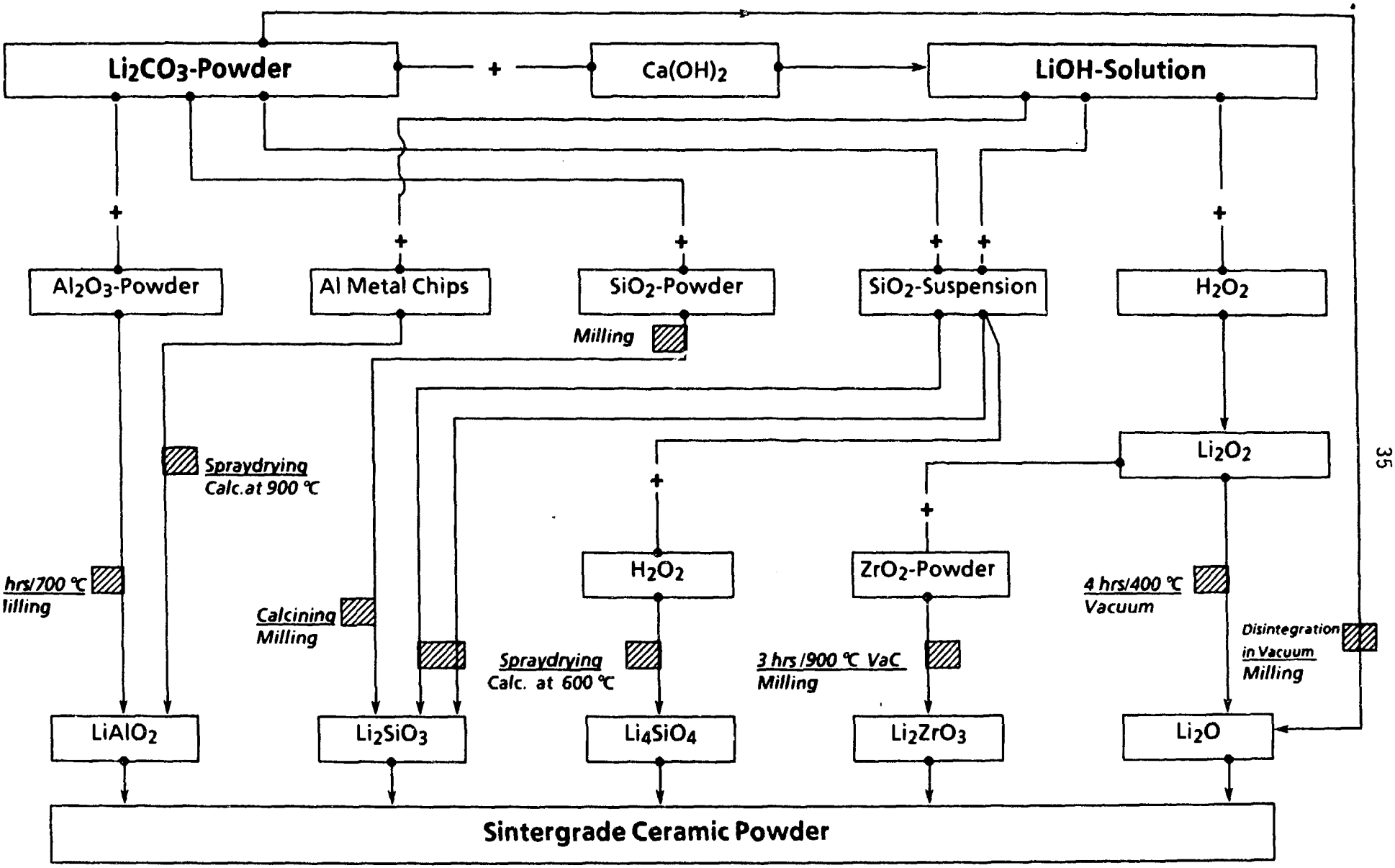

Fig. 2. The Preparation of Sinter-Grade Lithium Ceramic Powders

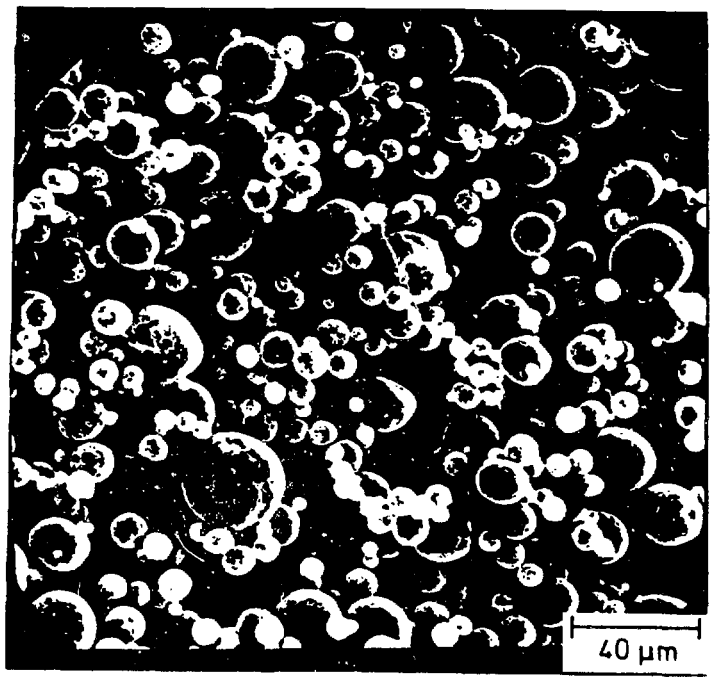

Fig. 3. Spray-dried Li_2SiO_3 Powder Produced from SiO_2 Suspension in LiOH Solution

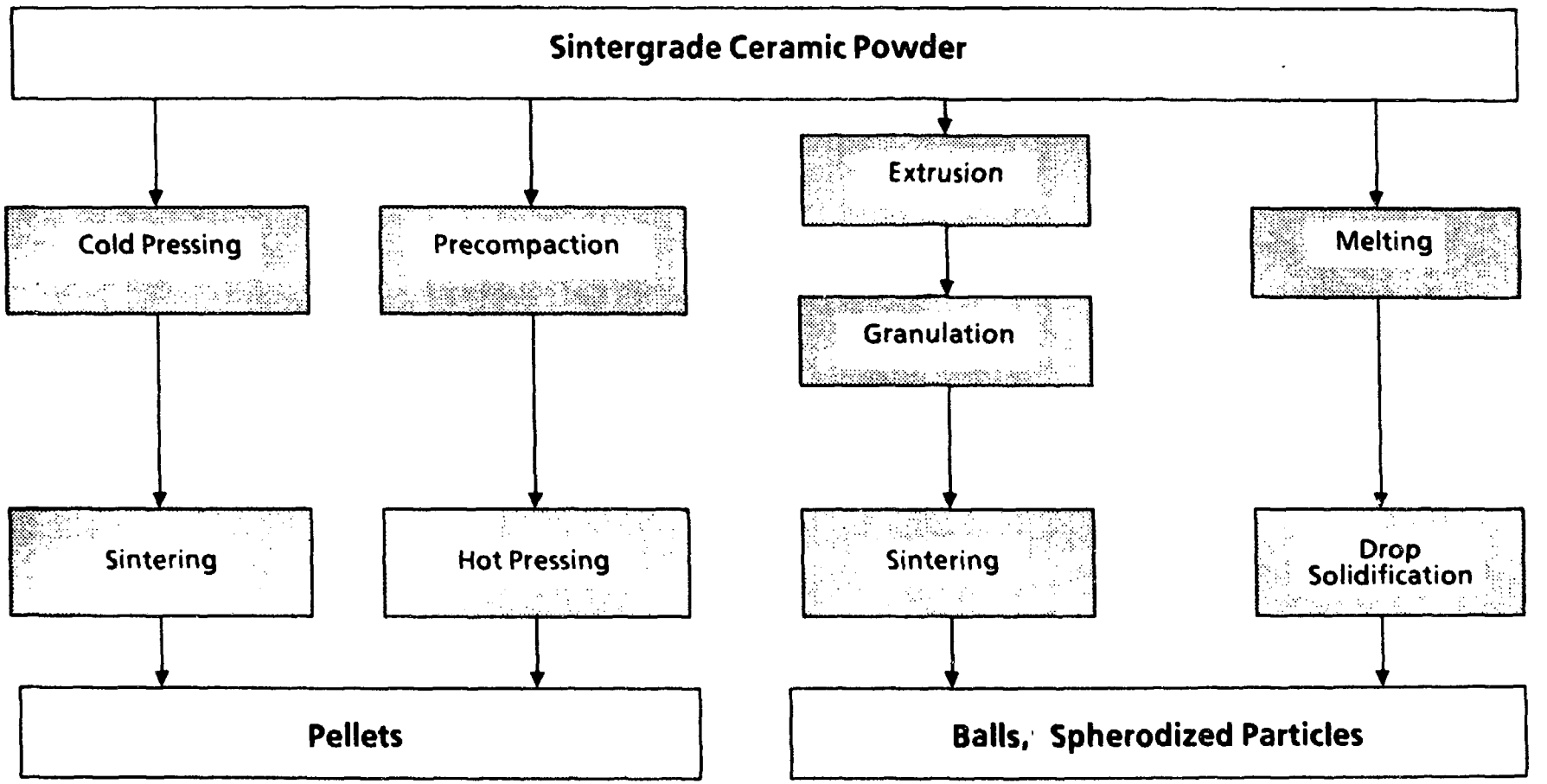

Fig. 4. The Condensation to Solids from Ceramic Powder

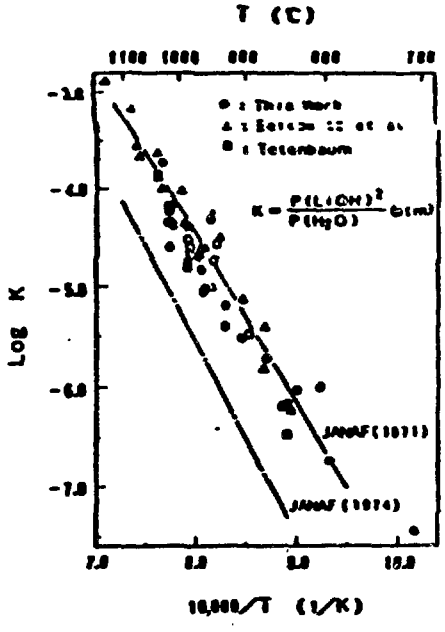

Fig. 5. Equilibrium Constants for the Reaction:
$Li_2O(s) + H_2O(g) \rightleftarrows 2LiOH(g)$

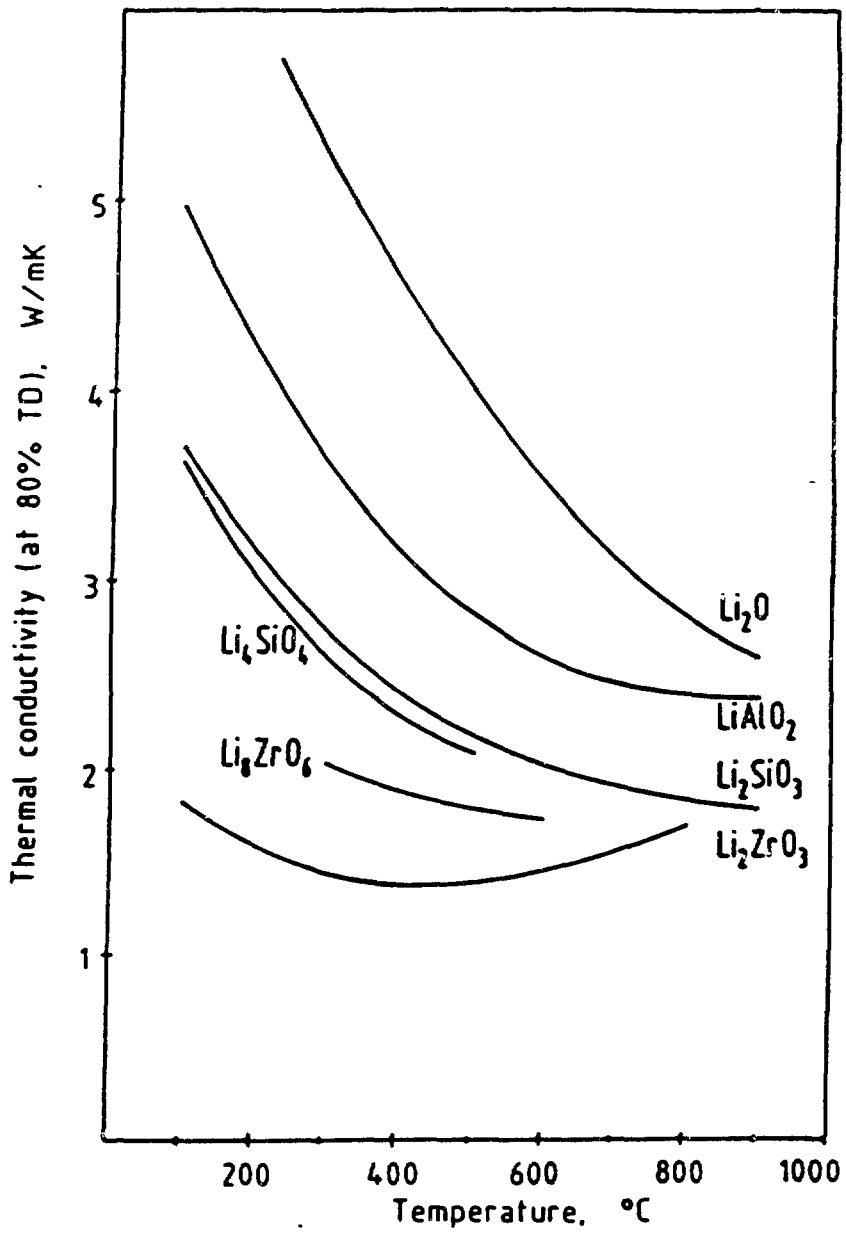

Fig. 6. Thermal Conductivity of Ceramic Breeder Materials (of 80% TD)

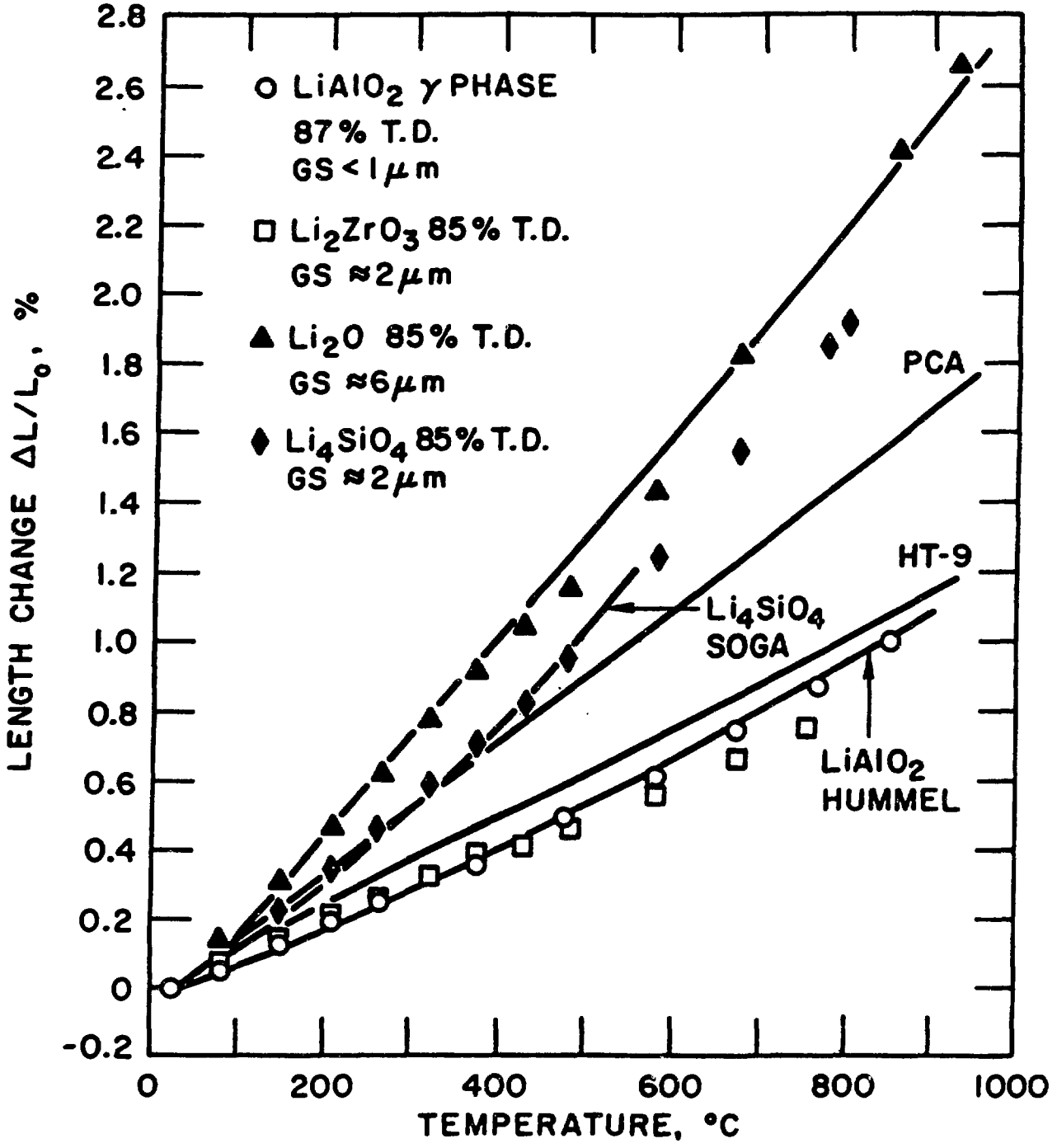

Fig. 7. Thermal Expansion of Solid Breeder and Structural Materials

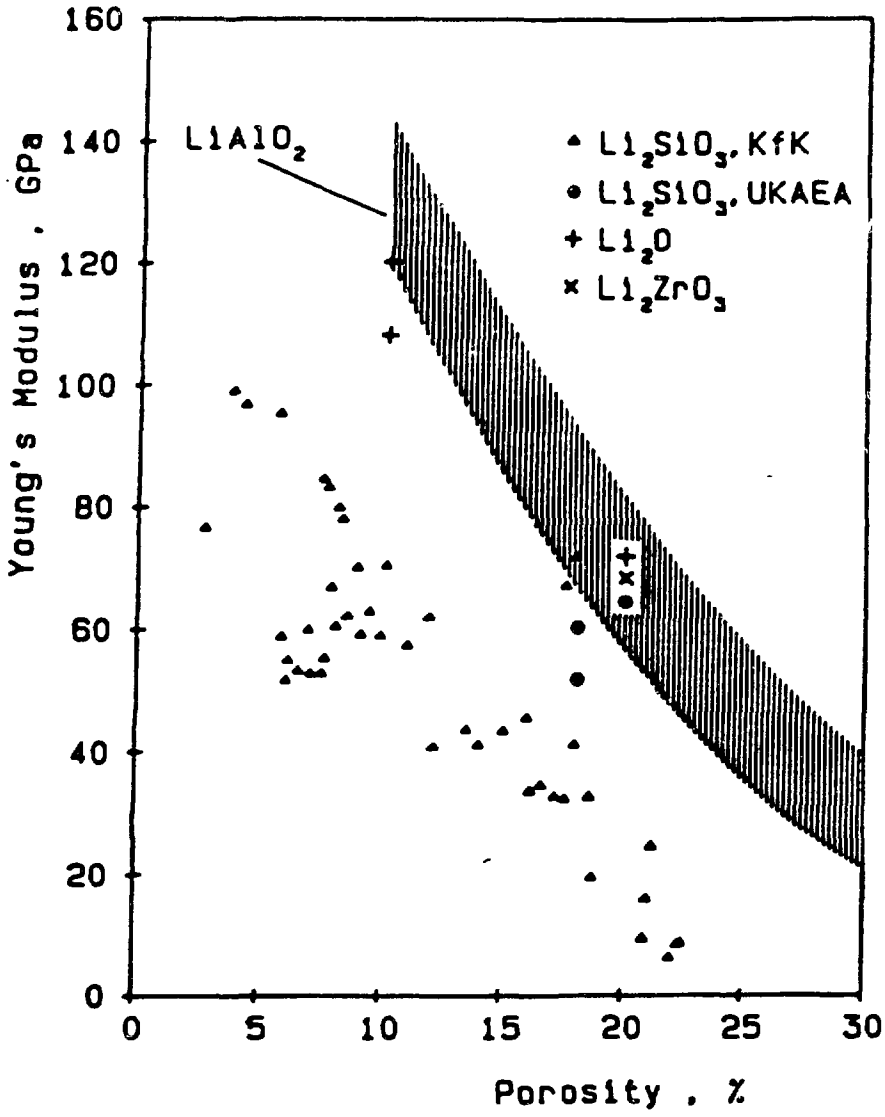

Fig. 8. Young's Modulus of Ceramic Breeder Materials

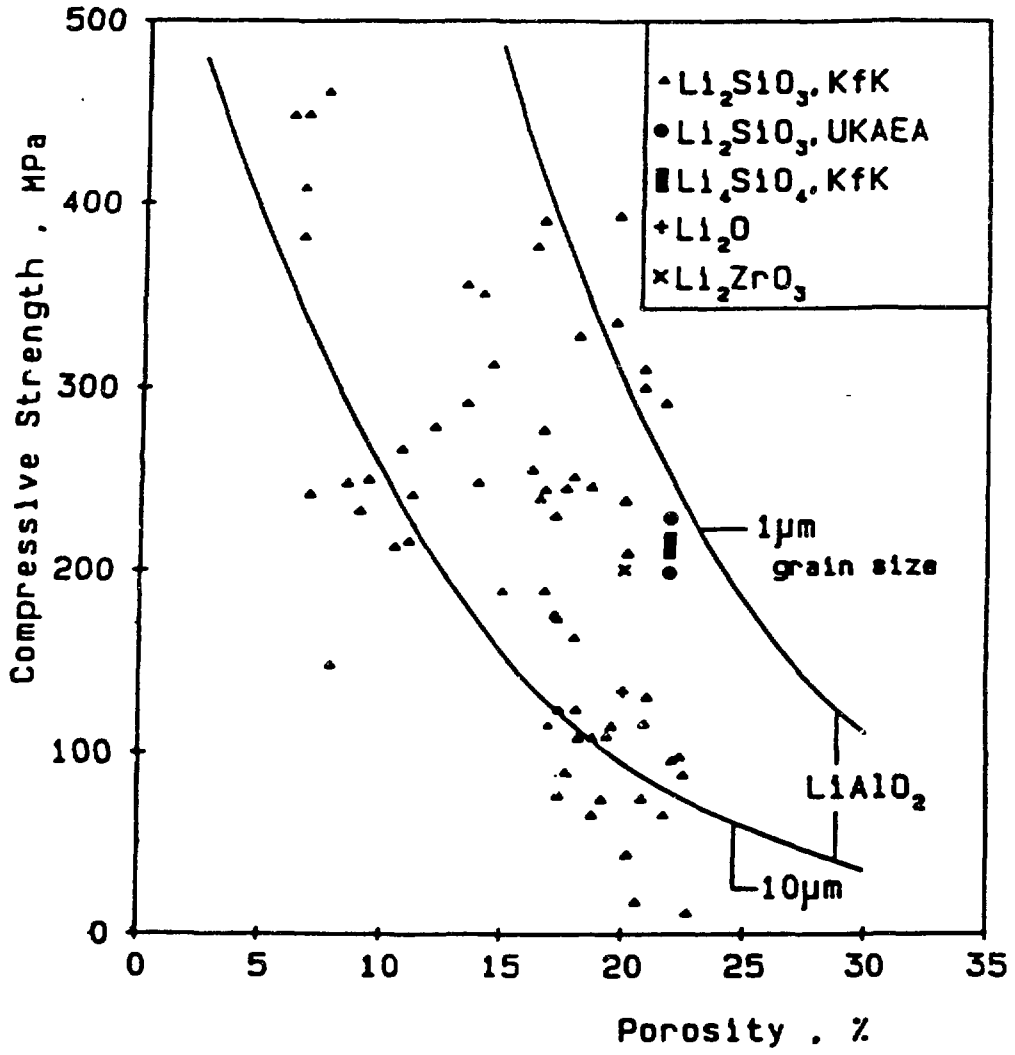

Fig. 9. Compressive Strength of Ceramic Breeder Materials

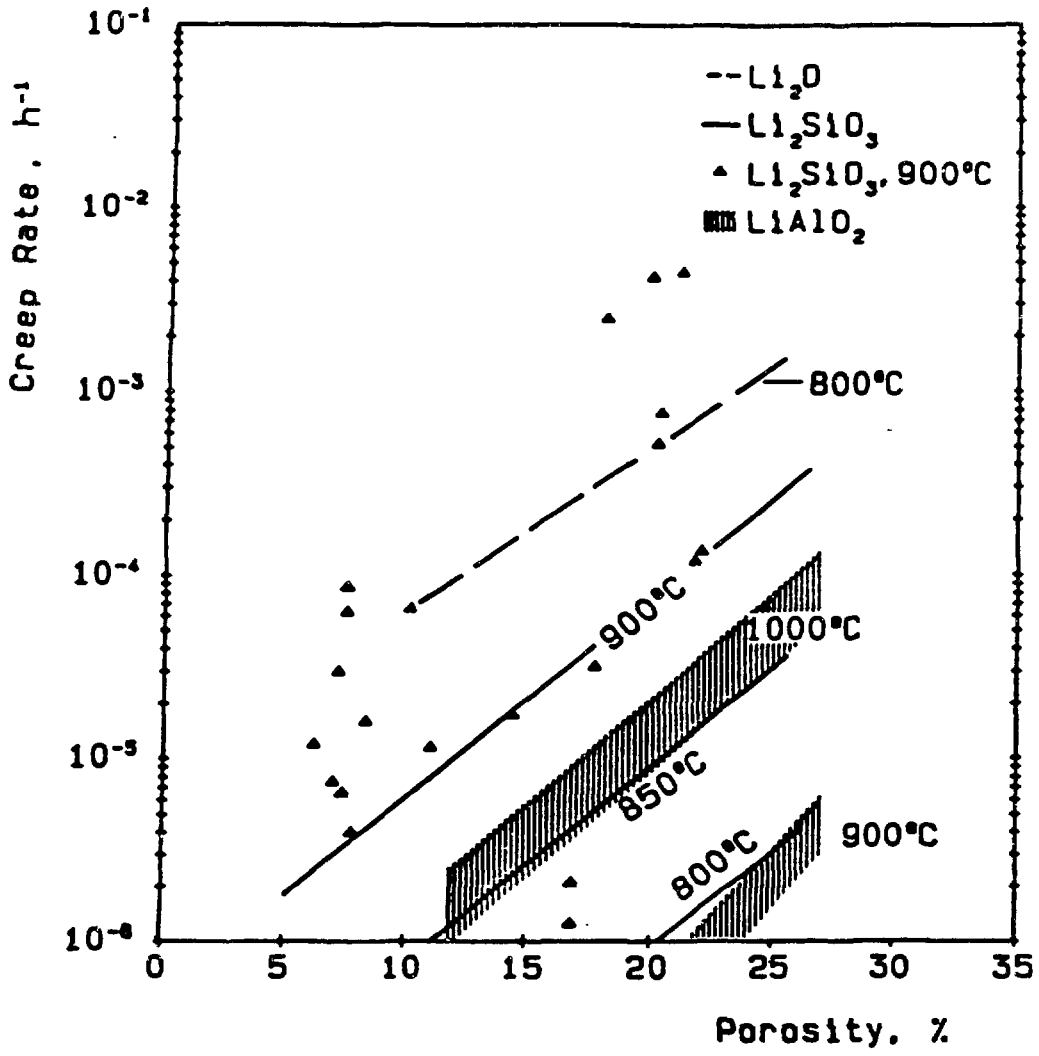

Fig. 10. Compressive Creep Rate of Ceramic Breeder Materials in 100 h at 10 MPa

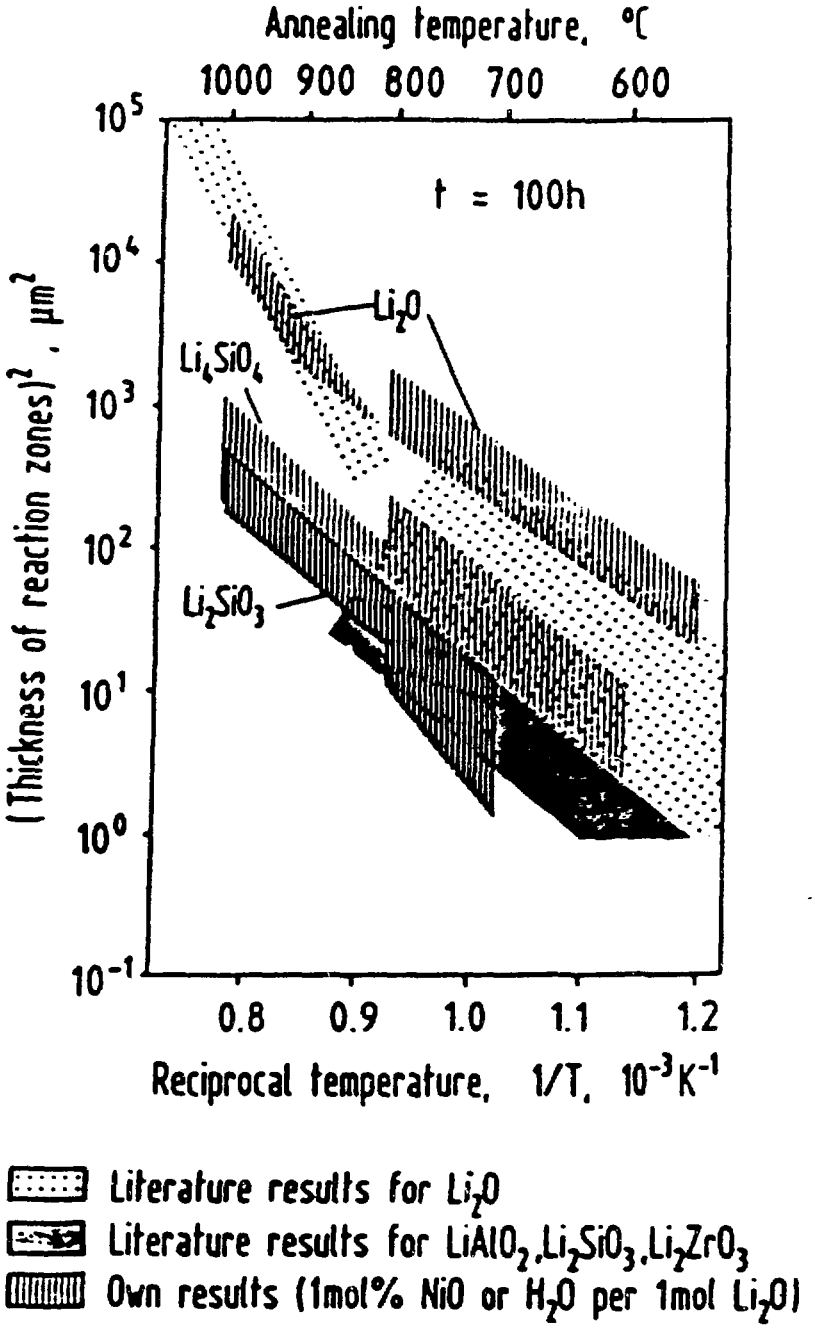

Fig. 11. Chemical Reaction of Li-Based Oxide Ceramics with Stainless Steels Normalized to 100 h

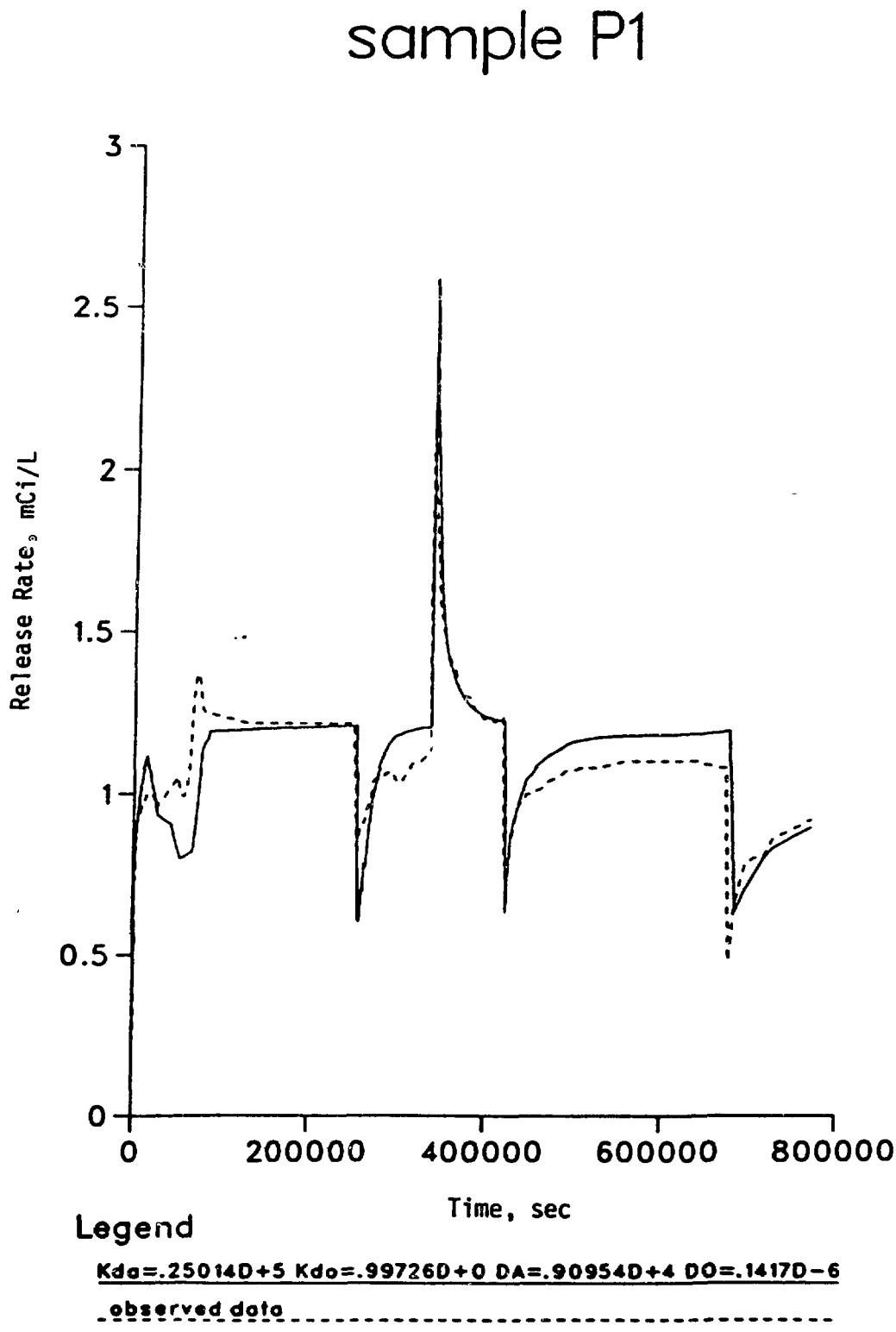

Fig. 12. Calculated and Observed Tritium Release Rate as Function of Time

DISCLAIMER